Petroleum 11 (2025) 601–612

Contents lists available at ScienceDirect

Petroleum

journal homepage: www.keaipublishing.com/en/journals/petlm

Full Length Article

Experimental study on the influence of heavy mud loss during workover on re-fracturing of high-pressure gas wells

Yuxuan Liu [a,*], Minghao Jiang [a], Jianchun Guo [a], Xinggui Yang [a], Jiamin Wu [b], Liansong Wu [a], Xiaopeng Chen [a], Zhiming Wen [c], Chuanyun Zhou [d]

[a] State Key Laboratory of Oil and Gas Reservoir Geology and Exploitation, Southwest Petroleum University, Chengdu 610500, China
[b] Sinopec Exploration Company, Chengdu 610041, China
[c] Oil and Gas Engineering Research Institute of PetroChina Tarim Oilfield Company, Korla, Xinjiang 841000, China
[d] Downhole Service Company, CNPC Chuanqing Drilling Engineering Company Limited, Chengdu, Sichuan, China

ARTICLE INFO

Article history:
Received 14 February 2025
Received in revised form
20 May 2025
Accepted 2 July 2025

Keywords:
High-pressure gas well
Workover
Refracturing
Heavy mud leakage
Loss medium

ABSTRACT

During workover operations in high-pressure gas wells, heavy mud losses may occur, reducing gas production. Refracturing is an effective means to restore production. The influence of heavy mud loss on refracturing is still unclear. In this paper, split core is designed to simulate the fractures of the initial transformation, transparent sand-filled pipe is designed to simulate the sand filled fractures, and the experiment of heavy mud leakage in artificial fractures under different conditions is carried out by using the displacement device, combined with CT scanning and pressure monitoring means. The influence of heavy mud loss on permeability of artificial fracture, repeated reconstruction construction pressure and flow channel configuration in artificial fracture is analyzed. The results show that workover heavy mud (WHM) loss has the greatest permeability damage to the proppant fracture packed with large particle size, up to 97%, and the fracture permeability damage of 40/70 mesh ceramsite packing is only 0.3%–0.7%. Slit core permeability damage is the least, and the decrease range is 10%–20%. The damage of matrix core permeability measured by gas is no less than 60%. Before and after the loss of WHM, the injection pressure increases significantly, up to 80 times. Combined with the CT scan results, it is found that after WHM loss, the nitrogen blowout and refracturing incompletely remove the pollution, and there is a "pollution cage" in the fracture, which is the main reason for the high construction pressure of refracturing and low production after refracturing. The research results provide theoretical basics for the refracturing of WHM loss wells.

1. Introduction

The Tarim Basin is the largest onshore oil and gas basin in China, and Kuqa piedmont is the key natural gas production area of Tarim oilfield. The fractured tight sand stone reservoirs in this area are characterized by burial depth (over 7000 m), high formation pressure (the maximum reservoir pressure exceeds 150 MPa), high formation temperature (120–190 °C), and low matrix porosity (porosity 4%–8%, permeability 0.01–0.1 × 10^{-3} μm^2). Reservoir reconstruction is the key technology to realize economical and efficient development because the natural productivity of a single well cannot meet the requirements of development and distribution. After the initial reconstruction, during the long-term production process of the gas well in Kuqa piedmont, the wellbore is faced with complex problems such as wax deposition, scaling and hydrate blockage, resulting in abnormal production of oil and gas wells, so well workover operations must be carried out [1,2]. However, the workover process faces the challenge of deep reservoir burial and high formation pressure. In order to achieve effective workover and kill operations, barite is often added to the workover fluid to improve the mud density [3]. The use of heavy mud workover will cause reservoir pollution, resulting in loss of production of a single well [4,5]. After workover, it is necessary to resume production through refracturing [6–9]. In the process of refracturing, some Wells have problems such as abnormal construction pressure and large difference in productivity after

* Corresponding author.
E-mail address: liuyx_6@163.com (Y. Liu).
Peer review under the responsibility of Southwest Petroleum University.

https://doi.org/10.1016/j.petlm.2025.07.002

fracturing. The workover operation procedure is complicated, and the solid particles in the heavy mud during workover will invade the reservoir and block the rock pores [10–13]. Combined with the comparative analysis of the data of the repeatedly reconstructed well polluted by heavy mud during workover, it is found that the heavy mud loss is the main reason (Table 1).

Most of the existing mud contamination experiments mainly focus on drilling mud, whose components are mainly water, bentonite, polymers, salts and other additives, in order to achieve the performance required for drilling. Mud leakage and intrusion into the reservoir will cause a series of adverse consequences. On the one hand, after the filtrate invents the stratum, it will form multi-point adsorption of organic polymers, water locking, rock wetting reversal, and cause clay hydration, expansion, dispersion and migration in water-sensitive strata, thereby reducing the permeability of the rock [14–19]. On the other hand, solid particles in the mud invade the reservoir and clog the pore space, which will also cause reservoir damage [20–24]. In 1995, Yu et al. [25] calculated the degree of mud intrusion into the core and the variation of its depth through a new type of instrument—the JHST permeability gradient meter without damaging the core, and found that the depth of mud intrusion in cores with different permeability was different. Subsequently, many scholars have also carried out a large number of mud dynamic filtration loss experiments and summarized the law of mud intrusion depth [26,27]. Based on this, a large number of scholars began to study the influence of different factors on the mud loss of natural fractures, including displacement pressure difference, fracture width and roughness [28,29]. In 2020, Guo et al. [30] conducted mud loss experiments on artificial split cores with different widths and different fracture surface roughness using a core displacement device. They found that when the fracture width was less than 150 μm, the mud could not pass through the fracture and a filter cake would form at the fracture mouth. The above scholars mainly judged the pollution characteristics of the mud by the amount of mud loss. In addition, many scholars evaluated the pollution characteristics of the mud by testing the changes in porosity, permeability and fracture conductivity of the core before and after the mud invasion [31,32]. In 2024, Mehdi Rahmati et al. [33] conducted mud invasion experiments on cored samples with fractures, and evaluated the changes in porosity, permeability and conductivity of the samples before and after the experiment. To more intuitively analyze the pore structure and fracture evolution of the rock samples before and after the mud invasion, scholars have also begun to conduct research at the microscale, including XRD testing, cast thin sections, scanning electron microscopy and CT scanning techniques [34–36]. In addition, scholars have also begun to study complex situations such as mud loss under drilling conditions through numerical simulation methods [37–40]. In 2023, Jin et al. [41] considered the time-varying characteristics of wellbore temperature and pressure and the distribution laws of fracture temperature and pressure, and established a coupled model of temperature and pressure in the wellbore and fractures. They used the finite difference approximation to numerically solve the developed model. The results showed that under high temperature and high pressure conditions, the performance of the mud would change significantly, which had a significant impact on mud loss. In 2024, Cai [42] and Jin [43] et al. incorporated the consideration of fracture morphology into the existing three-dimensional fracture reservoir drilling fluid leakage model, further improving the leakage rules of drilling fluid in fractured formations.

For the simulation experiments of construction pressure, most scholars adopt the true triaxial physical simulation method for research [44]. Studies have shown that the injection pressure and its peak fracture pressure are significantly influenced by the viscosity of the fracturing fluid, the flow rate, the permeability of the rock, and the mechanical properties of the rock [45–47]. In 2023, Huang et al. pre-embedded a fracture in a cubic cement specimen to simulate the old fracture from the initial fracturing process. They then conducted true triaxial repeated fracturing experiments to study the influence of the old fracture on the expansion of the new fracture. The results showed that there was a stress interference phenomenon when the new fracture ruptured, causing the pressure within the old fracture to increase rapidly. The longer the old fracture and the smaller the fracture spacing, the greater the rupture pressure and expansion pressure of the new fracture [48]. Some scholars have also conducted mud-soaking experiments to study the impact of mud filtrate invasion on the mechanical properties of rocks [49]. Furthermore, Ding et al.'s research indicates that the shape of the fracturing fractures, as well as the presence of fillers within the fractures, also have a significant impact on the construction pressure [50].

Overall, the existing research on drilling mud pollution is mainly based on standard core columns and cored fractured cores (simulating matrix pores and natural fractures) [51], and analyzed through displacement experiments combined with electron microscopy, CT scan, and other means. However, the loss of workover heavy mud occurs after fracturing treatment, and the loss medium has expanded to three types: matrix, shear self-supporting fractures, and propped fractures (Fig. 1). Currently, there is no systematic comparative study on these three media. Experimental methods are also limited by rock sample preparation and device functions, making it difficult to fully simulate the on-site operation process of “heavy mud loss - well opening and blowout - repeated fracturing”, and unable to reflect the impact of heavy mud loss after the initial treatment. Therefore, this study uses an improved displacement experiment device, simulating shear self-supporting fractures and propped fractures through cored fractured cores and cored propped fractured cores respectively, to focus on studying the dynamic influence law of heavy mud loss on the injection pressure during repeated fracturing.

To clarify the influence of heavy mud loss during well workover on the repeated fracturing operation, taking the tight sandstone reservoir in the front of the Kuqa Mountains in Tarim as the research object, the heavy mud samples used on site were collected, and the parameters such as mud density, mud specific gravity and solid content were analyzed and tested. Based on the

Table 1
Statistics of workover heavy mud contamination and refracturing in Kuqa piedmont.

No	Open flow rate before workover (10^4 m^3/d)	Open flow rate after workover refracture (10^4 m^3/d)	Construction pressure before workover (MPa)	Refracture pressure after workover (MPa)	Heavy mud loss (m^3)
Well 1	12.77	20.44	77.9–117.6	65.0–112.6	0
Well 2	190.00	59.06	46.2–105.7	76.3–132.1	13
Well 3	61.76	87.65	59.5–118.0	95.0–108.0	0
Well 4	13.03	26.85	94.0–100.0	90.0–115.0	0

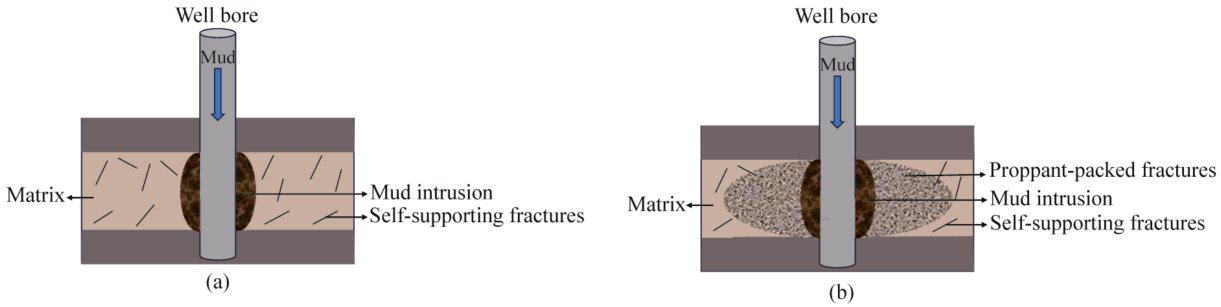

Fig. 1. Schematic diagram of the medium for heavy mud loss: (a) Drilling mud loss medium; (b) Workover mud loss medium.

core displacement experimental device, the field procedures of heavy mud loss - well opening and blowdown - repeated treatment were simulated for matrix, shear self-supporting fractures and propped fractures. The indoor physical simulation was carried out to analyze the characteristics of mud pollution, clarify the relationship between injection pressure and heavy mud pollution, and observe the changes in the distribution of flow channels in the fractures by CT scanning to reveal the reasons why heavy mud pollution affects productivity and operation pressure. The main workflow of this study is shown in Fig. 2.

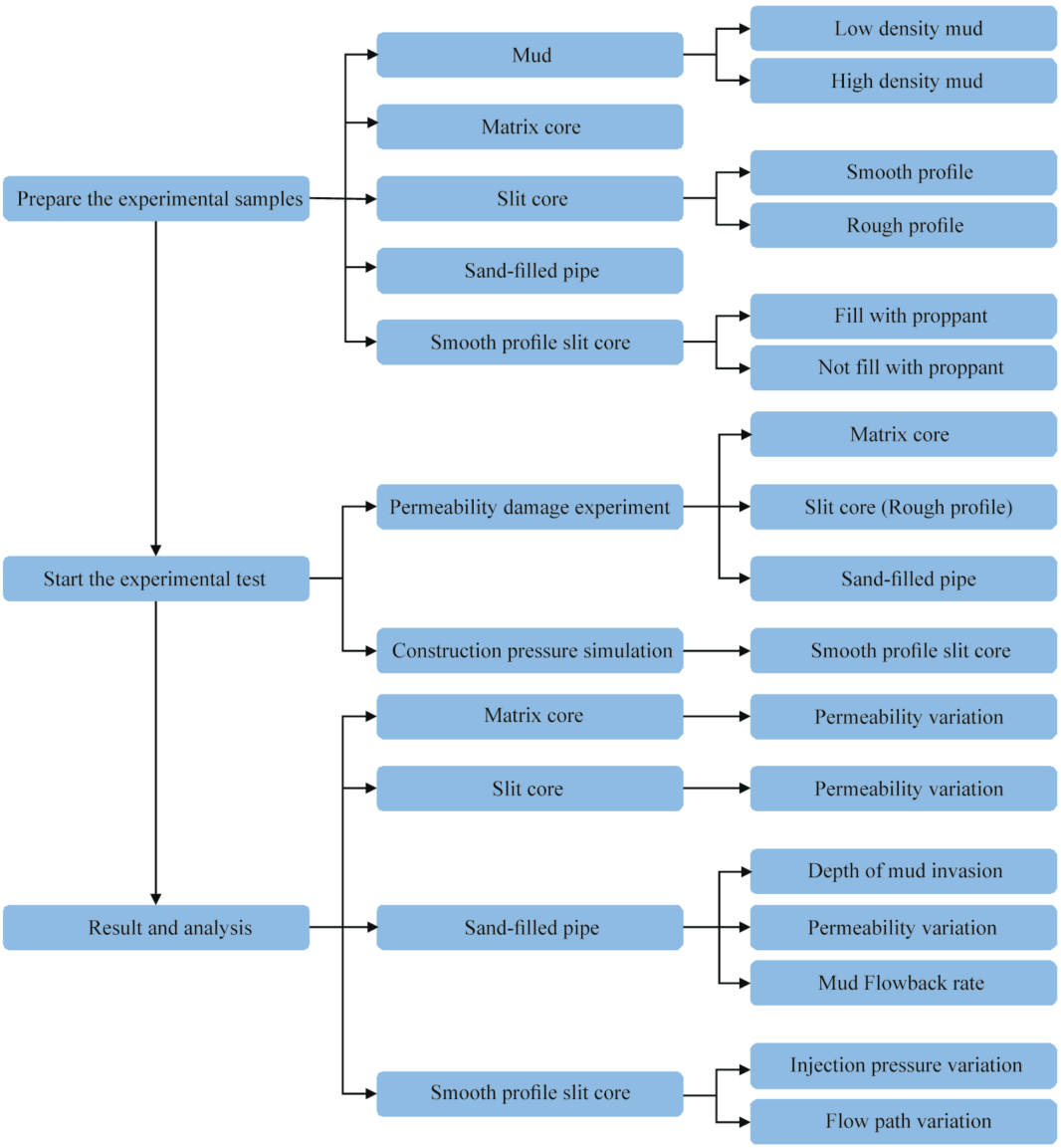

Fig. 2. Outline of research workflow.

2. Experimental design

2.1. Experimental sample

Low-density and high-density mud samples were selected from the well repair site in front of the Kuqa Mountain. Tests were conducted on their density, solid content and mineral composition. The results are shown in Fig. 3. The densities measured in the laboratory were 1.34 g/cm^3 and 2.26 g/cm^3 respectively, and the solid contents were 56.36% and 76.52% respectively. Both were mainly composed of barite.

The matrix pore samples were made using standard core columns, as shown in Fig. 4(a). Self-supporting fracture samples were made using split cores, as shown in Fig. 4(b), to simulate acid-fracturing/acid-pressurized fractures or shear-slip natural fractures. To study the influence characteristics of mud invasion on propped fractures, a pressure-resistant transparent sand-filled tube was fabricated, as shown in Fig. 4(c). The sand-filled tube was 27 cm long with an inner diameter of 0.98 cm and a maximum pressure resistance of 10 MPa. The filling material was ceramic proppant, as shown in Fig. 4(e). Smooth-surfaced artificial cut core slices were made, as shown in Fig. 4(d). The ceramic proppant was filled in the core to simulate sand-filled fractures. The two ends of the core were sealed with gauze to prevent the proppant from leaking out, and finally the core sides were fixed with heat shrinkable tubes.

Fig. 3. Experimental mud samples.

2.2. Experimental equipment

The experimental equipment (Fig. 5) includes: ISCO high-precision pumps (displacement pumps and peripheral pressure pumps), data recording systems (recording flow and pressure data), intermediate containers (storing displacement fluid), pressure gauges, core clamps (supporting matrix cores and fracture cores), pressure-bearing transparent sand filling pipes (simulating proppant filling fractures), nitrogen sources (providing reverse displacement pressure) The testing equipment includes core porosity, ultra-low permeability combined testing system and CT scanning equipment, etc., such as simulating the blowout process in the mine and measuring cylinders (for collecting liquids).

2.3. Experimental method

2.3.1. Permeability damage experiment

This study conducted permeability damage experiments using a core displacement device. The experimental setup is shown in Fig. 5. Three types of core samples were used: matrix core Fig. 4 (a), fractured core Fig. 4(b), and propped fracture core Fig. 4(c). For the matrix core permeability damage experiments, the effects of heavy mud loss on the permeability of matrix cores were analyzed from three factors: displacement pressure, displacement time, and displacement fluid type. A total of 10 experiments were conducted, and the experimental plan is shown in Table 2. The permeability was measured using the BenchLab 7000-HPHT instrument before and after the experiments. For the shear self-supporting fracture permeability damage experiments, the research was carried out under different confining pressures and mud densities, with a total of 6 experiments. The experimental plan is shown in Table 3 For the propped fracture permeability damage experiments, the research was conducted under different proppant particle sizes, displacement pressures, and mud types, with a total of 6 experiments. The experimental plan is shown in Table 4. The experimental process is shown in Fig. 6.

2.3.2. Injection pressure and flow channel variation experiment

To study the influence of mud contamination on injection pressure and flow channels within fractures in sand-filled and self-supporting fractures, in order to eliminate the impact caused by different roughness of each core section, smooth core sections were used for the experiment. The experimental samples are shown in Fig. 4(b) (unfilled core) and Fig. 4(e) (core filled with proppant). The fracture width of the core was set at 0.6 mm. The experimental setup is shown in Fig. 5, and the experimental plan is presented in the Table 5. The experimental process is shown in Fig. 7.

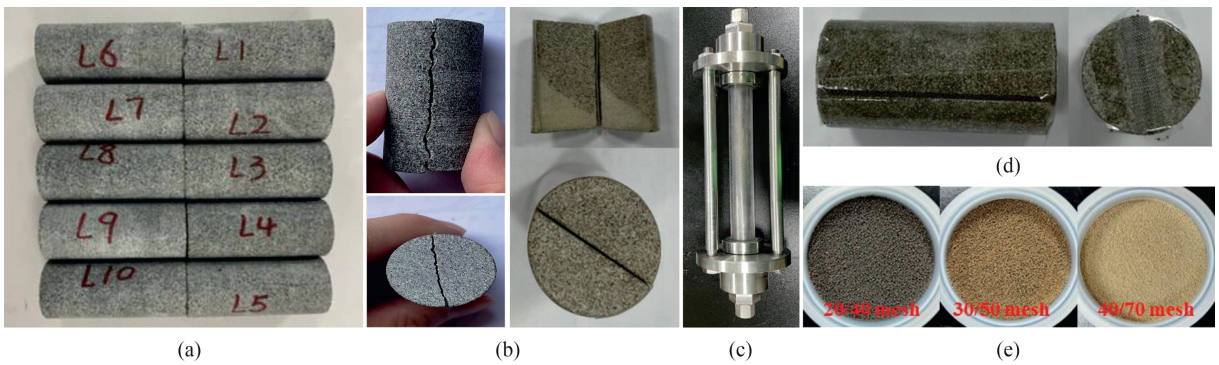

Fig. 4. The materials used in the experiment: (a)matrix core; (b)split core (rough section and smooth section); (c) experimental proppant-pack pipe; (d)split-packed core; (e) ceramsite proppant.

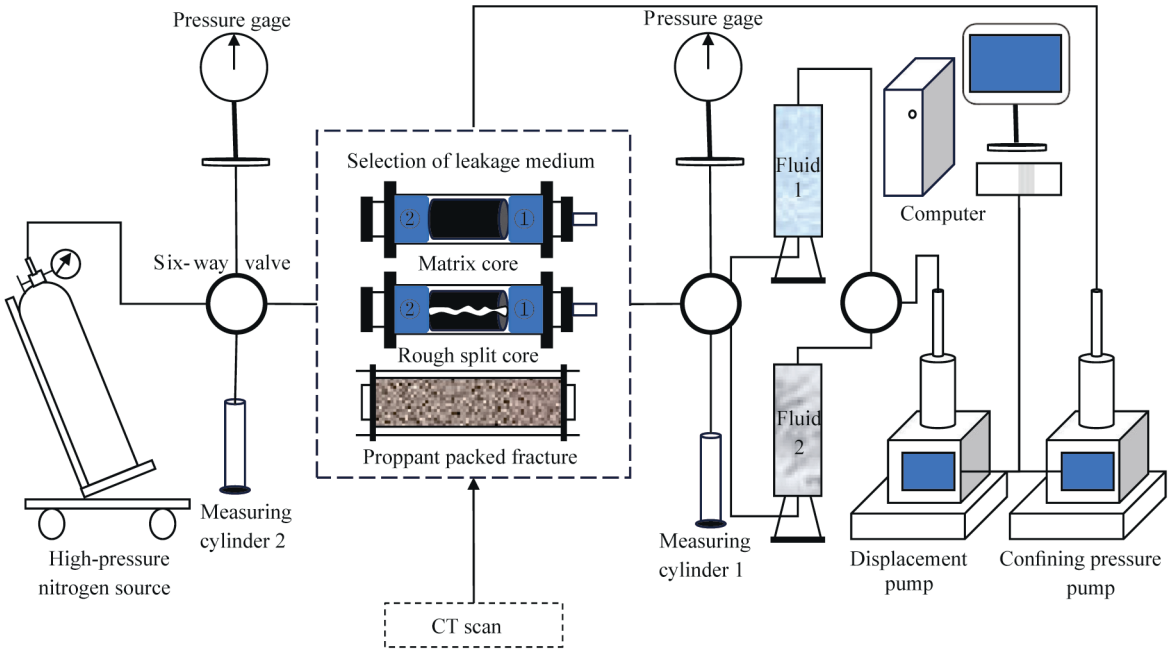

Fig. 5. Schematic diagram of experimental apparatus.

Table 2
Experimental scheme of matrix core damage.

No	Core No.	Displacement pressure (MPa)	Time (min)	Confining pressure (MPa)	Displacement fluid
1	L1	2	40	10	LDM
2	L2	2	80	10	
3	L3	2	120	10	
4	L4	4	120	10	
5	L5	6	120	10	
6	L6	2	40	10	HDM
7	L7	2	80	10	
8	L8	2	120	10	
9	L9	4	120	10	
10	L10	6	120	10	

3. Experimental results and analysis

3.1. Experimental results and analysis of permeability damage

3.1.1. Matrix core

Fig. 8 shows the impact of mud invasion on the permeability of matrix cores. Experimental data indicate that after the core is invaded by mud, the permeability significantly decreases, with the overall damage degree being no less than 60%. Specifically, low-density mud causes more severe damage to the core compared to high-density mud. Under the action of low-density mud, the damage to the core gradually intensifies as the displacement time increases; when the displacement time exceeds 80 min, the rate of permeability reduction begins to slow down. The damage

Table 3
Experimental scheme of permeability damage of shear self-supported fracture.

No.	Forward displacement pressure (MPa)	Reverse displacement pressure (MPa)	Confining pressure (MPa)	Forward time (min)	Reverse time (min)	Forward displacement fluid	Reversedisplacement fluid
1	2	3.5	5	To be stable fluid	30	Water	LDM
2			7				
3			9				
4			5				HDM
5			7				
6			9				

Table 4
Experimental scheme of permeability damage of proppant-packed fracture.

No	Proppant size (mesh)	Positive displacement pressure (MPa)	Positive displacement time (min)	Reverse displacement pressure (MPa)	Positive displacement time (min)	Mud type
1	40/70	1、3、5、7	30	1	5	LDM
2						HDM
3	30/50					LDM
4						HDM
5	20/40					LDM
6						HDM

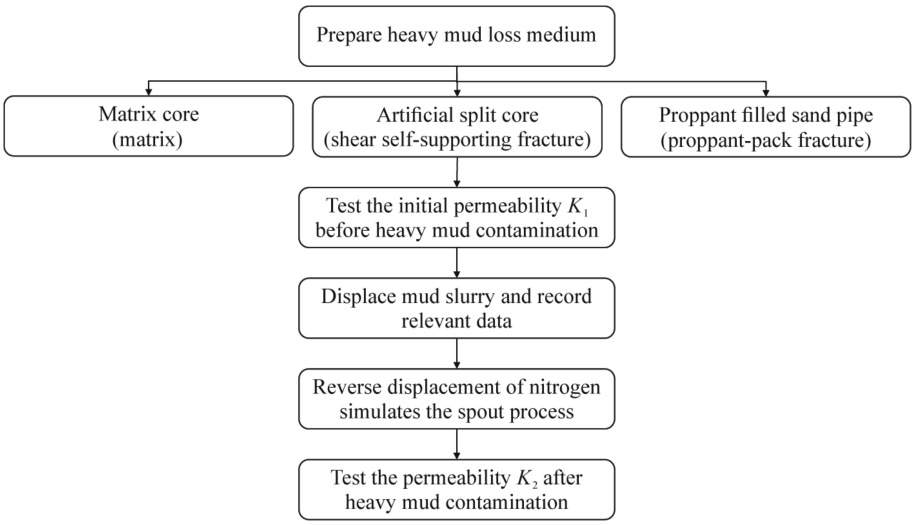

Fig. 6. Permeability damage experiment procedure.

Table 5
Experimental parameter design.

No	Fracture width (mm)	Fracture Filler	Confining pressure (MPa)	Displacement (mL/min)	Displacement fluid	fracturing fluid
1	0.6	30/50 mesh ceramsite	20	1	LDM	Slick water
2				2		
3				3		
4		Nothing		1		
5				2		
6				3		

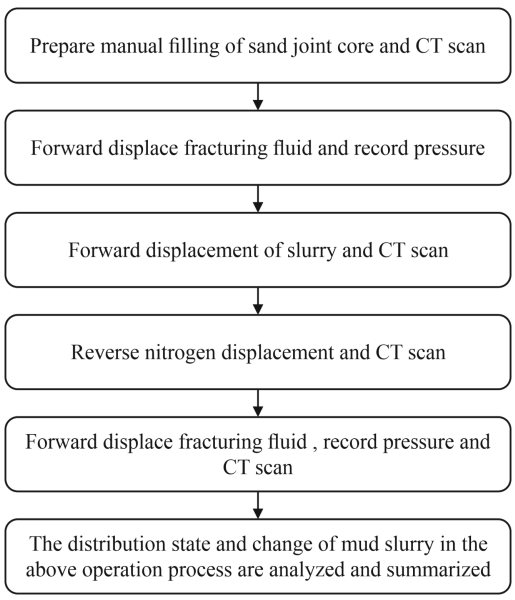

Fig. 7. Experimental flow of fracture injection pressure and flow channel distribution changes before and after mud contamination.

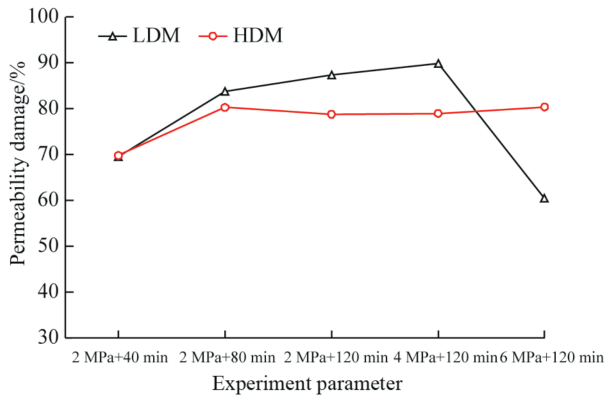

Fig. 8. The influence of mud intrusion on the permeability of the matrix core.

characteristics of high-density mud to the core are similar to those of low-density mud.

Regarding the variation in displacement pressure, when the displacement pressure gradually increases from 2 MPa to 6 MPa, the damage to the core permeability caused by high-density mud is relatively minor, with the overall damage rate remaining at approximately 80%. Under the displacement pressures of 2 MPa and 4 MPa, the damage characteristics of low-density mud to the core are similar to those of high-density mud; however, when the displacement pressure increases to 6 MPa, the damage rate of core permeability caused by low-density mud decreases instead, reaching only 60.4%. Fig. 9 presents the physical image of the matrix core after being contaminated by mud, where a relatively thick mud cake forms on the end face of the core.

To further clarify the damage characteristics of the matrix core caused by mud pollution, the core L5 and L10 were continuously and automatically scanned before and after mud pollution using the core scanning system to obtain the permeability changes along

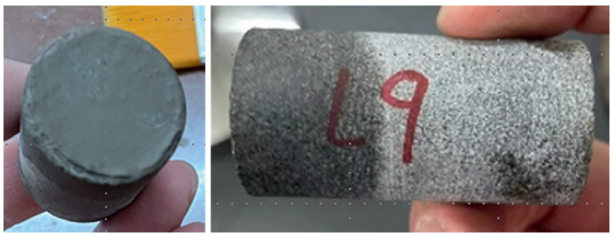

Fig. 9. A physical picture of the core after mud contamination.

the length of the matrix core. The gas permeability of 8 linear regions on the side surface of the core was scanned, with a phase angle of 90°. The Auto-Scan core automatic scanner used in the experiment is shown in Fig. 10.

Fig. 11 shows the permeability scanning results of each point on the core before and after mud contamination. The results indicate that the contamination range of the core after the invasion of low-density mud is close to 30 mm, while that of high-density mud is close to 25 mm, which is smaller than that of low-density mud.

3.1.2. Slit core

Fig. 12 shows the results of the impact of mud invasion on the permeability of self-supporting fractures. The results indicate that mud invasion causes a certain degree of damage to the permeability of self-supporting natural fractures. The liquid permeability of the core before and after mud contamination decreases by 10%–20%. With the increase of confining pressure, the permeability change does not show a monotonous trend, and its fluctuation mainly results from the difference in the surface roughness of the core fractures created by artificial splitting. During displacement, mud preferentially invades along the local high-conductivity channels, leading to significant differences in the damage to the permeability of self-supporting fractures among different experimental groups. Fig. 13 shows the physical images of the cored samples before and after mud contamination.

3.1.3. Sand-filled pipe

The invasion depth of mud in the proppant-packeded tube was used to characterize the mud loss in the proppant-packeded fractures, and the mud loss volume is positively correlated with the degree of contamination. To facilitate the summary of

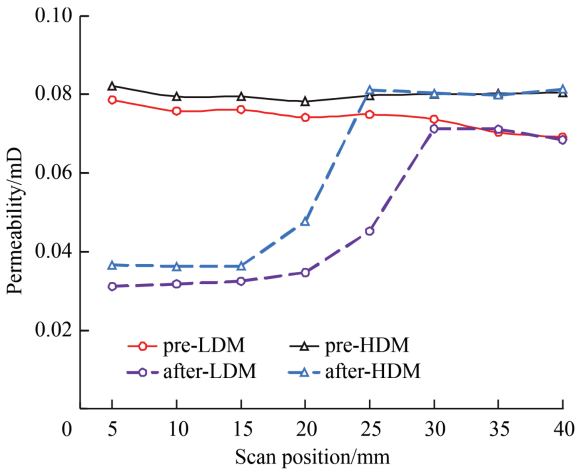

Fig. 11. The results of core permeability scanning experiments before and after mud contamination (displacement pressure is 6 MPa, time is 120 min).

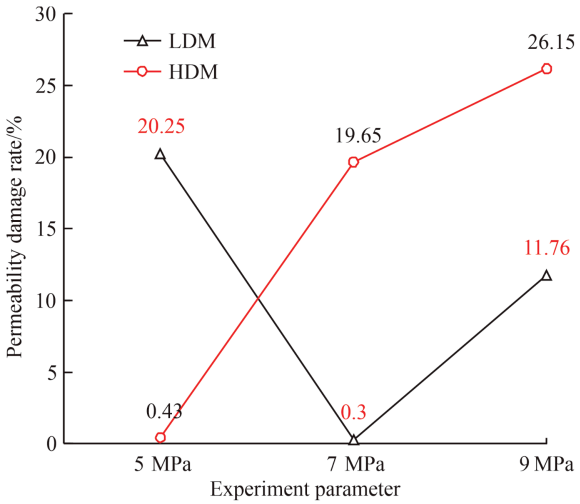

Fig. 12. The influence results of mud pollution on the permeability of self-supporting fractures.

(a)

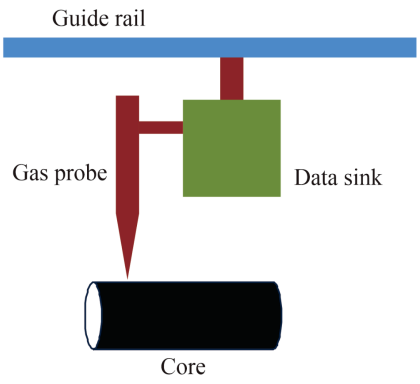

(b)

Fig. 10. Core permeability scanning device: (a)profile Display; (b)device schematic diagram.

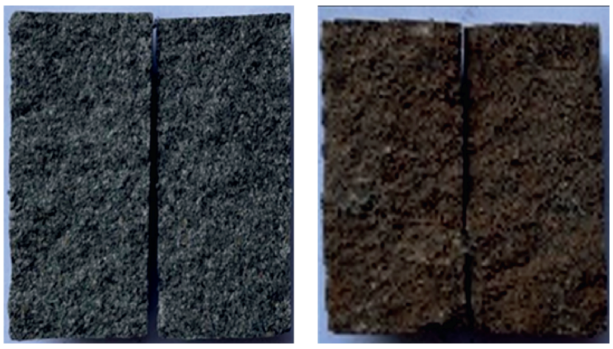

Fig. 13. Core images of the fracture before and after mud contamination.

experimental laws, the experimental results were dimensionless, and the calculation formula was as follows:

$$D = \frac{V_2}{V_P} \cdot L \tag{1}$$

$$D^* = \frac{D}{D_{max}} \tag{2}$$

where D is the actual invasion depth of mud, cm; V_2 is the outflow volume at port ②, mL; V_P is the pore volume of the proppant accumulation in the proppant-packeded pipe, cm^3; D^* is the dimensionless mud invasion depth, dimensionless; D_{max} is the maximum invasion depth in 6 groups of experiments, cm.

The pore volumes of 40/70 mesh, 30/40 mesh and 20/40 mesh compact deposits in proppant filled pipes were calculated by constant velocity and constant flow pump, respectively, to be 8.75 cm^3, 11.13 cm^3 and 13.23 cm^3.

Permeability is an important index to judge the seepage capacity of fluid. Based on Darcy's law to process the pressure and flow data recorded by the data recording system, the permeability before and after mud intrusion into the proppant filling pipe is calculated and dimensionless processing is done. When the fluid passes through the proppant filling pipe, its flow rate is directly proportional to the cross-sectional area of the proppant body in the proppant filling pipe and the pressure difference between the inlet and outlet section, and inversely proportional to the length of the proppant body. The calculation formula is as follows:

$$Q = K\frac{A\Delta P}{\mu L} \times 10^{-1} \tag{3}$$

Simplifed as:

$$K = \frac{Q\mu L}{A\Delta P} \times 10 \tag{4}$$

Dimensionless:

$$K^* = \frac{K}{K_{max}} \tag{5}$$

where, Q is displacement pump displacement,mL/s; A is proppant pipe cross-sectional area,cm^2; ΔP is displacement pressure,MPa; μ is viscosity of clean water, mPa·s; L is proppant pack length in proppant packed pipe,cm; K is permeability,10^{-3} μm^2; K_{max} is highest permeability of all test groups,10^{-3} μm^2; K^* is dimensionless permeability, dimensionless.

During workover, the effective return of mud can reduce damage to the reservoir. In the experiment, the calculation formula for the mud return rate is as follows:

$$F = \frac{V_1}{V_2} \times 100\% \tag{6}$$

where F is mud flowback rate,%; V_1 is port ① liquid output; V_2 is port ② liquid output。

In the experimental results shown in Fig. 14 and Fig. 15, the penetration depth of the mud and the changes in the permeability of the propped fractures within the sand-filled pipe during the displacement process, as well as the mud return effect, were statistically analyzed. The results indicate that the distance (D^*) that the mud penetrates into the sand-filled fractures is jointly controlled by three factors: mud density, proppant particle size, and displacement pressure. The specific rules are as follows.

Overall, low-density mud, large proppant particle size, and high displacement pressure result in a deeper penetration of the mud into the sand-filled fractures. Specifically, at a relatively low displacement pressure (1 MPa), the penetration depth of low-density mud and high-density mud is relatively similar. As the displacement pressure increases, the penetration depth of high-density mud changes little across the three proppant particle sizes, while the penetration depth of low-density mud increases significantly. However, in the fractures filled with small proppant particles, further increasing the displacement pressure does not lead to a significant change in the penetration depth of low-density mud, and the penetration depths of both densities of mud are comparable and remain at a relatively low level. The difference in penetration depth between the two densities of mud caused by the displacement pressure decreases as the proppant particle size decreases.

For sand-filled fractures, the mud return rate and the permeability damage rate before and after mud contamination are most affected by the particle size of the proppant, while the density of the mud has a relatively minor impact. When the proppant particle size is small, the mud has a relatively small impact on the permeability of the supported fracture, with a reduction rate ranging from 0.03% to 1.1%, and the mud return rate after nitrogen blowout is 100%. As the proppant particle size increases, the permeability of the supported fracture after mud contamination is extremely low, with a damage rate of over 97%, and the mud return rate is low, with an average return rate of 23.9%.

Further analysis reveals that as the proppant particle size increases, the pore space within the sand-filled pipe increases, providing more space for fluid flow. The initial permeability of the sand-filled pipe is greater, and the mud is more likely to flow within the pipe, with a greater invasion depth. During the early stage of pumping, there is more pore space within the sand-filled

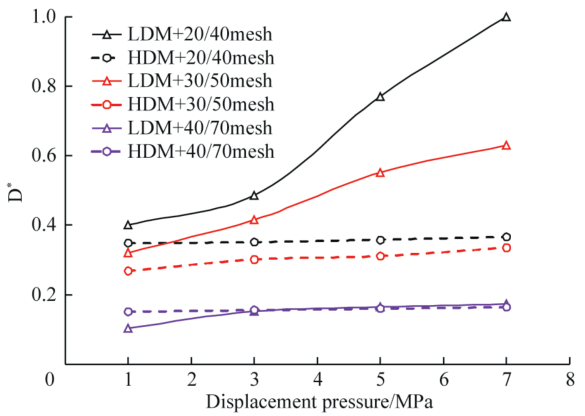

Fig. 14. Dimensionless intrusion depth varies with displacement pressure.

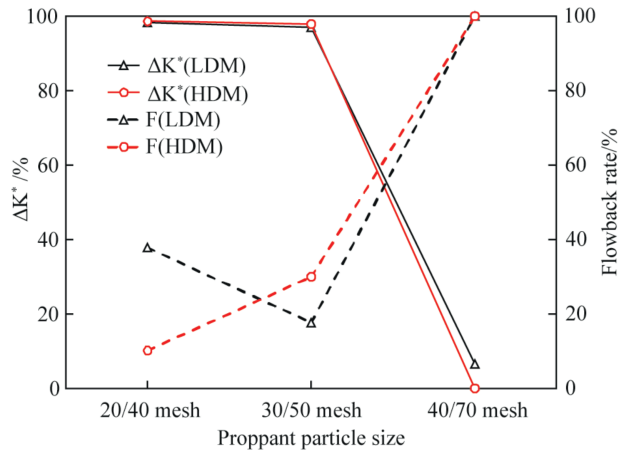

Fig. 15. Effect of mud intrusion on permeability of proppant-packed fractures.

pipe, and high-density mud shows an invasion volume comparable to that of low-density mud. Due to the higher solid content in high-density mud, it quickly occupies the pore space, blocking the flow channels, making subsequent mud pumping difficult and resulting in a smaller invasion volume. Moreover, during nitrogen reverse displacement, it is difficult to expel the mud that has invaded the sand-filled pipe, leading to a low mud return rate.

3.2. Experimental results and analysis of injection pressure and flow channel changes

When the mud is not contaminated, the injection pressure of clear water in the shear self-supporting fractures is stable, ranging from 0.12 to 1.19 MPa, and the injection pressure of clear water in the propped fractures is between 0.07 MPa and 0.42 MPa. Fig. 16 shows the injection pressure change curves before and after heavy mud contamination. The results indicate that after the fractures are contaminated by heavy mud, the pressure required to pump fracturing fluid into the fractures at the same flow rate increases significantly. The average increase in injection pressure for shear self-supporting fractures is 17 times, with a maximum increase of 74 times; for propped fractures, the average increase is 16.5 times, with a maximum increase of 80 times. The injection pressure of fracturing fluid in shear self-supporting fractures fluctuates more intensely than that in propped fractures.

Specifically, after mud contamination, the injection pressure curve of fracturing fluid in shear self-supporting fractures can be divided into four stages (taking the injection pressure change curve of shear self-supporting fractures at a flow rate of 3 mL/min as an example): (1)initial low-pressure stable stage (0–200 s), the pressure is stable in the range of 0.8–1.2 MPa. After blowout, local areas of the fracture form dominant flow channels, and the fracturing fluid passes through rapidly. The flow resistance is mainly determined by the inherent structure of the fracture. The duration of this stage is negatively correlated with the flow rate (about 300 s at 1 mL/min and about 200 s at 3 mL/min). A high flow rate accelerates the migration of mud particles, triggering the next stage; (2)pressure surge stage (200–400 s), the pressure rapidly rises from 1.2 MPa to 8 MPa, an increase of more than 6 times. This is because the solid particles in the mud migrate and bridge in the fracture, blocking the flow channels and causing a significant increase in pressure; (3)pressure fluctuation stage (400–1000 s), the pressure fluctuates periodically between 8 and 11 MPa. When the pressure reaches a certain value, due to the weak structural stability of the temporary blockage area, the fracturing fluid breaks

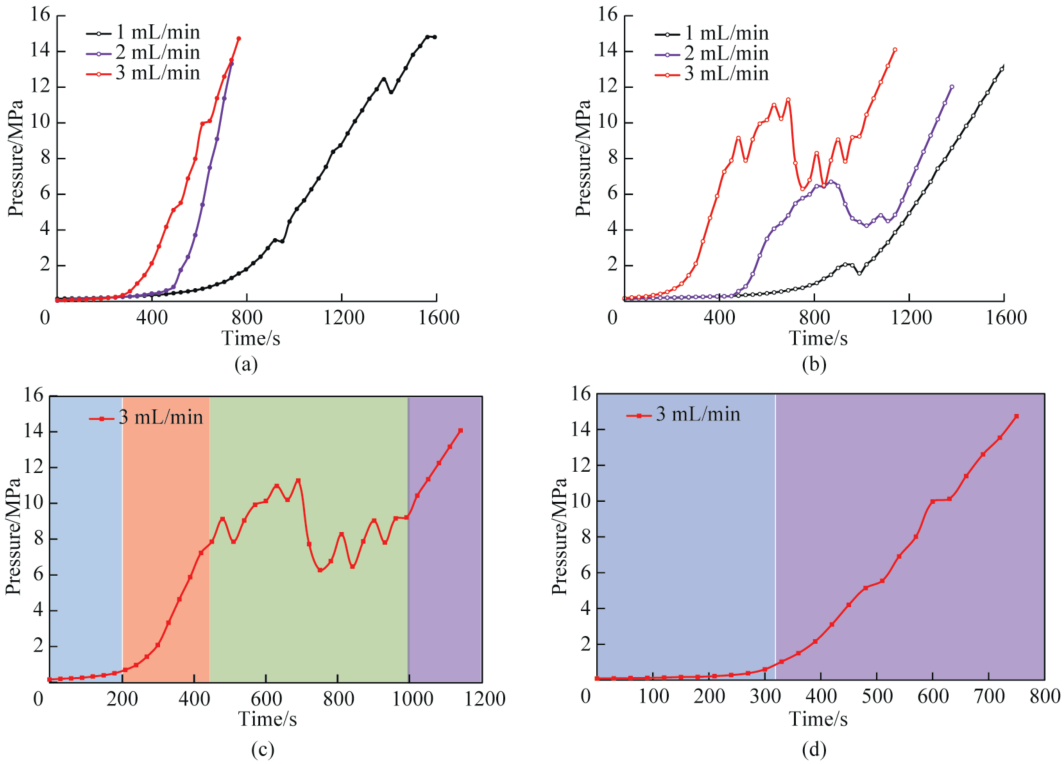

Fig. 16. The injection pressure variation curves after mud contamination: (a)the injection pressure variation curves of shear self-supporting fractures under different displacements; (b)the injection pressure variation curves of sand-filled fractures under different displacements; (c)the injection pressure variation curves of shear self-supporting fractures under a displacement of 3 mL/min; (d)the injection pressure variation curves of sand-filled fractures under a displacement of 3 mL/min.

through the blockage, and the pressure drops rapidly. The particles continue to migrate, forming a cycle of self-organized particle blockage and breakthrough; (4)pseudo-steady-state blockage stage (1000–1200 s), the pressure continuously rises to 14 MPa, and the fluctuation amplitude decreases. As the fracturing fluid is continuously injected, the remaining solid particles in the mud are eroded and migrate, eventually accumulating in the fracture to form a relatively stable blockage area, causing the pressure to continuously rise. The injection pressure curve of fracturing fluid in propped fractures can be divided into two stages (taking the injection pressure change curve of propped fractures at a flow rate of 3 mL/min as an example): (1)initial low-pressure stable stage (0–300 s), the pressure is stable in the range of 0.5–0.8 MPa; (2) pressure increase stage (300–800 s), the pressure linearly increases from 0.8 MPa to 15.2 MPa. Compared with shear self-supporting fractures, the injection pressure of fracturing fluid in propped fractures after heavy mud contamination has smaller fluctuations. This is because the propped fractures are filled with proppants evenly, and after the heavy mud invades, the fracturing fluid exerts a compaction effect on the proppant sand piles and mud solid particles. The injection pressure curve initially rises relatively gently and then increases rapidly.

The CT scan results (Fig. 17) show that after the fracture was contaminated by mud, the entire fracture surface was almost uniformly distributed with high-brightness barite signals, indicating that the solid particles in the heavy mud almost invaded the entire fracture. After the reverse displacement of nitrogen gas to simulate blowout, black areas were clearly visible within the fracture surface, representing that the solid particles in these areas were affected by the blowout and moved. After the repeated fracturing, the black areas within the fracture did not change significantly. Most of the fracturing fluid flowed along the channels blown out by the blowout, indicating that the fractures formed during the initial modification were the channels for the loss of heavy mud and the inflow of fluids during the repeated modification. The repeated fracturing failed to establish new seepage channels and could not remove the mud contamination.

The pollution characteristics of heavy mud loss during well workover are different from those of conventional drilling mud loss. There exists a phenomenon of “WHM loss pollution cage” (Fig. 18): after heavy mud loss occurs during well workover, the mud in the initially created artificial fractures has not been removed. The fluid will mainly flow along the space not occupied by the mud. When re-fracturing, the fracturing fluid is difficult to bypass the heavy mud pollution zone, ultimately resulting in high operation pressure and low post-fracturing productivity.

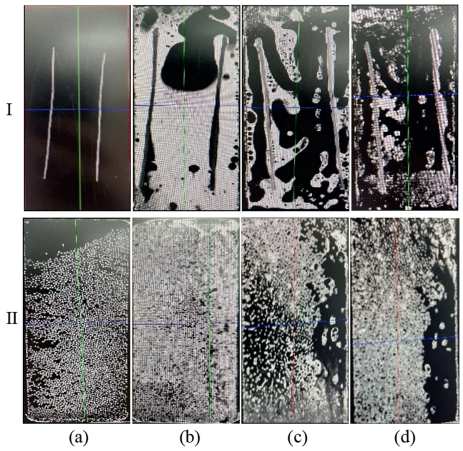

Fig. 17. CT scan results of fractures at each stage (I is shear self-supporting fracture, II is sand-filled fracture):(a) before pollution; (b)after pollution; (c)reverse nitrogen injection; (d)refracturing.

4. Discussion

This paper has conducted experimental research on the pollution characteristics of mud in different media. There are still two aspects that need to be further explored: (1) This paper mainly reveals the dominant mechanism of the increase in injection pressure caused by solid particle blockage. However, the abnormal pressure in the field during repeated fracturing is actually the result of the coupling of solid-liquid-force multiple fields. Mud loss not only involves solid phase invasion but also accompanies the physical and chemical interaction between filtrate and rock (such as clay hydration expansion and cement dissolution), which reduces the mechanical strength of the rock [52]. The change in injection pressure is the result of multiple factors, so the pollution characteristics of mud still need further study. (2) Although this paper uses the mud formula used in the field and considers the influence of displacement time, displacement pressure, and confining pressure on the experimental results, there are still differences from the actual underground conditions. The fractured and modified section is in a high-temperature and high-pressure environment, and the rheological properties of the liquid [53] and the properties of the rock samples will change, which has a certain impact on the experimental results. Therefore, the comparison between the results of indoor experiments and those under actual formation conditions needs further exploration.

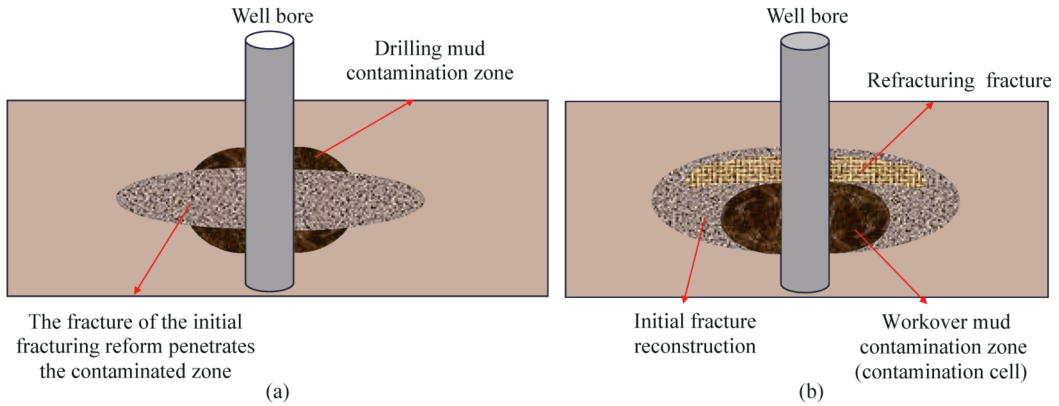

Fig. 18. Schematic diagram of fracturing transformation: (a) shows the initial fracture; (b) refracturing.

5. Conclusions

The first systematic experimental study was conducted on the leakage pollution characteristics of the wellbore heavy mud after the initial modification. Three leakage media of the wellbore heavy mud were identified: matrix, shear self-supporting fractures and propped fractures. The influence of heavy mud leakage on the permeability of the leakage media was discussed, and the injection pressure and the distribution of the flow channels in the fractures after heavy mud pollution were analyzed. The main conclusions are as follows:

(1) For the matrix core, the matrix permeability damage after mud invasion exceeds 60%, and the damage caused by low-density mud is higher than that of high-density mud. The invasion depth of the mud shows a “threshold effect”, and even if the displacement pressure or time is increased, the invasion depth and damage rate tend to be stable.
(2) The permeability of shear self-supporting fractures decreases by 10%–20% after mud invasion, but the data are scattered due to the difference in fracture surface roughness, and no clear pattern is presented.
(3) The degree of propped fracture pollution is dominated by the particle size of the proppant. The larger the particle size, the lower the mud return efficiency and the more severe the permeability damage.
(4) The solid particles of heavy mud blockage cause a sharp increase in injection pressure when the fracturing fluid is pumped repeatedly. The average injection pressure of shear self-supporting fractures and propped fractures increases by 17 times and 16.5 times respectively, and the peak values reach 74 times and 80 times respectively, indicating that solid blockage is the direct cause of abnormal pressure in field operations.
(5) The CT scan results reveal the “wellbore mud pollution cage” phenomenon: the initial fractures are the main channels for leakage and repeated fracturing fluid injection. If the pollution is not removed, the fluid bypasses the unpolluted area, making it difficult for repeated fracturing to penetrate the pollution zone.

CRediT authorship contribution statement

Yuxuan Liu: Funding acquisition, Writing – original draft, Writing – review & editing. **Minghao Jiang:** Writing – review & editing, Writing – original draft. **Jianchun Guo:** Funding acquisition, Methodology. **Xinggui Yang:** Methodology, Formal analysis, Validation. **Jiamin Wu:** Methodology, Formal analysis. **Liansong Wu:** Writing – Review & Editing. **Xiaopeng Chen:** Data curation. **Zhiming Wen:** Data curation. **Chuanyun Zhou:** Data curation.

Data availability

Data will be made availability on request.

Declaration of competing interest

The authors declare that they have no known competing financial interests or personal relationships that could have appeared to influence the work reported in this paper.

Acknowledgements

This paper was supported by the National Natural Science Foundation Enterprise Innovation and Development Joint fund of China (No.U23B6004).

References

[1] D. Liu, R. Sun, Y. Zhang, Y. Wang, G. Li, A low density micro-foam workover fluid for deep and ultra-deep wells with low-pressure coefficient and high inorganic salt, Colloids Surf. A Physicochem. Eng. Asp. 682 (5) (2024) 132870, https://doi.org/10.1016/j.colsurfa.2023.132870.
[2] X. Zheng, J. Shi, G. Gao, N. Yang, M. Cui, D. Jia, Progress and prospects of oil and gas production engineering technology in China, Petrol. Explor. Dev. 49 (3) (2022) 644–659, https://doi.org/10.1016/S1876-3804(22)60054-5.
[3] H. Al-Ziyadi, N. Kumar, A. VermaCA, Impact of cydroxypropyl cuar polymer on sheology and filtration properties of water-based drilling fluids, Petroleum (2025), https://doi.org/10.1016/j.petlm.2025.03.006.
[4] R.L. Arscott, New directions in environmental protection in oil and gas operations, J. Petrol. Technol. 41 (4) (1989) 336–342, https://doi.org/10.2118/17569-PA.
[5] Z. Yan, C. J. Okere, X. Zeng, et al., Preventing sour gas kicks during workover of natural gas wells from deep carbonate reservoirs with anti-hydrogen sulfide fuzzy-ball kill fluid, Energy Sci. Eng. 10 (8) (2022) 1, https://doi.org/10.1002/ese3.1158.
[6] Shi Wenrui, Li Jianfeng, Huang Zisang, Feng Yijiang, Hong Pu, Lei Shaojia, Wu Yi, Jianliang Wang, Meiyu Guo, Refracturing shale gas wells in China: poubling water consumption for enhanced gas recovery, Sci. Total Environ. 946 (2024) 174407, https://doi.org/10.1016/j.scitotenv.2024.174407.
[7] Yujie Wang, Zhao Bing, Zhennan Zhang, Numerical simulation of stress reorientation around wellbore in production and refracture stimulation, Eng. Anal. Bound. Elem. 133 (2021) 165–176, https://doi.org/10.1016/j.enganabound.2021.09.005.
[8] Mu Lijun, Li Xiangping, Yu Wenfeng, et al, Research on the optimal proportions of the new and old fractures in refracturing of horizontal wells in ultra-low permeability reservoirs, Petrol. Drill. Tech., 51(3) (20223),97-104. DOI:10.11911/syztjs.2023065.
[9] Wang Cong, Huang Shijun, Zhao Fenglan, et al., Reservoir evaluation method for refracturing in shale gas reservoir based on fast marching method, Fault-Block Oil Gas Field 30 (6) (2023) 940–946, https://doi.org/10.6056/dkyqt202306008.
[10] Necmettin Mungan, Permeability reduction through changes in pH and calinity, JPT (J. Pharm. Technol.) 17 (12) (1965) 1449, https://doi.org/10.2118/1283-PA.
[11] S.S. Rahman, C. Marx, Laboratory evaluation of formation damage caused by drilling fluids and cement slurry, J. Can. Petrol. Technol. 30 (6) (1991) 40–46, https://doi.org/10.2118/91-06-04.
[12] N.I. Ismail, E. Lawrence, M.Y. Naz, S. Shukrullah, S.A. Sulaiman, Role of particle size distribution of bridging agent for drilling mud on formation damage near wellbore, Mater. Today Proc. 47 (Suppl) (2020) S13–S17, https://doi.org/10.1016/j.matpr.2020.04.371.
[13] Li Jia, Xiong Ying, Yadong Zhang, Lan Ke, A novel self-healing and degradable plugging material for high temperature gas well, J. Mol. Liq. 376 (2023) 121473, https://doi.org/10.1016/j.molliq.2023.121473.
[14] Willis C. Cunningham, Dwight K. Smith, Effect of salt cement filtrate on subsurface formations, JPT (J. Pharm. Technol.) 20 (3) (1968) 259–264, https://doi.org/10.2118/1920-PA.
[15] Michael J. Economides, Kenneth G. Nolte, Reservoir Stimulation, 3rd Edition, John Wiley & Sons, 2009, p. 856.
[16] Li Jian, Ji Yuxi, Xiaoxiao Ni, Kaihe Lv, Xianbin Huang, Jinsheng Sun, A microcrosslinked amphoteric hydrophobic association copolymer as high temperature-and salt-resistance fluid loss reducer for water based drilling fluids, Pet. Sci. 21 (3) (2024) 1980–1991, https://doi.org/10.1016/j.petsci.2024.01.021.
[17] K.A. Fattah, A. Lashin, Investigation of mud density and weighting materials effect on drilling fluid filter cake properties and formation damage, J. Afr. Earth Sci. 17 (2016) 345–357, https://doi.org/10.1016/j.jafrearsci.2016.02.003.
[18] Y. Ye, C. Jihua, W. Jijun, et al., Experimental study on improving filtration properties of drilling fluid using silica nano-particles, Oil Drill. Prod. Technol. 35 (3) (2023) 30–41, https://doi.org/10.13639/j.odpt.2013.03.010.
[19] Imtiaz Ali, Maqsood Ahmad, Najeebullah Lashari, Optimizing filtration properties of water based drilling mud systems using dually modified starch, J. Clean. Prod. 454 (2024) 142022, https://doi.org/10.1016/j.jclepro.2024.142022.
[20] Zoran Krilov, Leopold Romic, Stojan Celap, Stevo Cabrajac, Permeability Damage Due to Precipitation of Insoluble Salts from Cement Slurry Filtrate, SPE International Symposium on Oilfield Chemistry, 1993, https://doi.org/10.2118/25218-MS.

[21] Nima Shojaei, Mohammad Hossein Ghazanfari, Reduction of formation damage in horizontal wellbores by application of nano-enhanced drilling fluids: experimental and modeling study, JPSE 210 (2022) 110075, https://doi.org/10.1016/j.petrol.2021.110075.
[22] Aghil Moslemizadeh, S. Shadizadeh, Minimizing water invasion into Kazhdumi Shale using nanoparticles, Iran. J. Oil Gas Sci. Technol. 4 (4) (2016) 15–32, https://doi.org/10.22050/ijogst.2016.12475.
[23] Erlong Yang, Yujia Fang, Liu Yongsheng, Li Zhengquan, Wu Jun, Research and application of microfoam selective water plugging agent in shallow low-temperature reservoirs, JPSE 193 (2020) 107354, https://doi.org/10.1016/j.petrol.2020.107354.
[24] Chinedum Peter Ezeakacha, Saeed Salehi, Experimental and statistical investigation of drilling fluids loss in porous media–part 1, J. Nat. Gas Sci. Eng. 51 (2018) 104–115, https://doi.org/10.1016/j.jngse.2017.12.024.
[25] Yu Weichu, Li Shulian, He Quan, A new method for evaluating the damage depth of drilling fluids and completion fluids to oil reservoirs - gradient analysis method, Drill. Fluids Complet. Fluids (5) (1995) 33–35.
[26] Li Fazhong, Ye Xianfang, Liu Gang, Gradient analysis, a new method to evaluate damaged reservoir depth by drill -in fluids, Drill. Fluids Complet. Fluids 21 (2) (2004) 29–31.
[27] J. Cai, Chenevert, et al., Decreasing water invasion into Atoka Shale using nonmodified silica nanoparticles, SPE Annual Technical Conference and Exhibition 27 (1) (2011) 103–112, https://doi.org/10.2118/146979-PA.
[28] Alexandre Lavrov, Johan Tronvoll, Modeling mud loss in fractured formations, Abu Dhabi International Conference and Exhibition, 2004, https://doi.org/10.2118/88700-MS.
[29] Lichu Jia, Chen, et al., Drilling fluid loss model and loss dynamic behavior in fractured formations, Petrol. Explor. Dev. 41 (1) (2014) 105–112, https://doi.org/10.1016/S1876-3804(14)60012-4.
[30] Jianchun Guo, Zhan, et al., Experimental optimization of acid system for acidizing in mud-damaged deep fractured carbonate formation, J. Petrol. Sci. Eng. 195 (2020) 107639, https://doi.org/10.1016/j.petrol.2020.107639 (Article).
[31] Karl Ronny Klungtvedt, Saasen, et al., A method for assessing drilling fluid induced formation damage in permeable formations using ceramic discs, J. Pet. Sci. Eng. 213 (2022) 110324, https://doi.org/10.1016/j.petrol.2022.110324.
[32] Badr Bageri, Jaber Al Jaberi, Abdulrauf R. Adebayo, et al., Understanding the complexity of secondary formation damage: mechanism and detection strategies during filter cake removal process, Geoenergy Sci. Eng. 231 (2023) 212287, https://doi.org/10.1016/j.geoen.2023.212287.
[33] Mehdi Rahmati, Mohamad Khosravi, Abbas Ayatizadeh TanhaCA, et al., Evaluation of formation damage and filter cake removal with a new LPM drilling fluid additive, Results Eng. 23 (2024) 102656, https://doi.org/10.1016/j.rineng.2024.102656.
[34] Hansen Sun, Chengwen Wang, Damage mechanism of cement slurry to CBM reservoirs with developed fractures and cleats: a case study from eastern Yunnan and western Guizhou in China, Nat. Gas. Ind. B 6 (2) (2019) 145–150, https://doi.org/10.1016/j.ngib.2018.09.004 (Article).
[35] Chengyuan Xu, Jirui Tang, Jinsheng Sun, et al., Dynamic stress sensitive analysis of fractured tight reservoirs under compound damage from drilling and fracturing fluids, Geoenergy Sci. Eng. 250 (2025) 213807, https://doi.org/10.1016/j.geoen.2025.213807.
[36] Aisan Rezaei, Shahab Ayatollahi, Vahid Khosravi, Pourya Malmir, Enhancing drilling efficiency: an experimental study on additives for mud loss mitigation in fractured media, Geoenergy Sci. Eng. 241 (2024) 213199, https://doi.org/10.1016/j.geoen.2024.213199.
[37] V. Nassehi, Modelling of combined Navier-Stokes and Darcy flows in cross-flow membrane filtration, Chem. Eng. Sci. 53 (6) (1998) 1253–1265, https://doi.org/10.1016/S0009-2509(97)00443-0.
[38] Mohd A. Kabir, Isaac K. Gamwo, Filter cake formation on the vertical well at high temperature and high pressure: Computational fluid dynamics modeling and simulations, J. Petrol. Gas Eng. 2 (7) (2011) 146–164, https://doi.org/10.5897/JPGE11.026.
[39] Saeed Salehi, Seyed Armin Madani, Raj Kiran, Characterization of drilling fluids filtration through integrated laboratory experiments and CFD modeling, J. Nat. Gas Sci. Eng. 29 (2016) 462–468, https://doi.org/10.1016/j.jngse.2016.01.017.
[40] Yuxuan Liu, Liansong Wu, Jianchun Guo, et al., Model for fracture conductivity considering particle size redistribution caused by proppant crushing, Geoenergy Sci. Eng. 240 (2024) 213081, https://doi.org/10.1016/j.geoen.2024.213081.
[41] An Jintao, Li Jun, Honglin Huang, Gonghui Liu, Hongwei Yang, Zhang Geng, Li Wentuo, Mud loss behavior in fractured formation with high temperature and pressure, Energy Rep. 9 (2023) 2638–2652, https://doi.org/10.1016/j.egyr.2023.01.080.
[42] Wenjun Cai, Li Zhong, Zhiming Yin, et al., Prediction of leakage pressure in fractured formation based on integration of geology and engineering, Fault-Block Oil Gas Field 31 (4) (2024) 676–683, https://doi.org/10.6056/dkyqt202404014.
[43] Taiyu Jin, Study on three-dimensional fluid-solid coupling model of drilling fluid leakage in rough fracture network, Petroleum Drilling Techniques 52 (1) (2024) 69–77, https://doi.org/10.11911/syztjs.2023100.
[44] Qiang Sun, Yifei Zhang, Chunlei Yu, et al., Experimental study on fracture initiation and propagation characteristics caused by pressure drive in low-permeability sandstone reservoirs, Petrol. Geol. Recov. Effic. 31 (6) (2024) 160–167, https://doi.org/10.13673/j.pgre.202307001.
[45] Li Minghui, Fujian Zhou, Jinjun Liu, Lishan Yuan, Guopeng Huang, Bo Wang, Quantitative investigation of multi-fracture morphology during TPDF through true tri-axial fracturing experiments and CT scanning, Pet. Sci. 19 (4) (2022) 1700–1717, https://doi.org/10.1016/j.petsci.2022.03.017.
[46] Tan Peng, Huiwen Pang, Jin Yan, Zhou Zhou, Experiments and analysis of hydraulic fracturing in hot dry rock geothermal reservoirs using an improved large-size high-temperature true triaxial apparatus, Nat. Gas Ind. B11 11 (1) (2024) 83–94, https://doi.org/10.1016/j.ngib.2024.01.002.
[47] Yushi Zou, Shicheng Zhang, Xinfang Ma, Xiaohuan Zhang, Shipeng Zhang, Hydraulic fracture morphology and conductivity of continental shale under the true-triaxial stress conditions, Fuel 352 (2023) 129056, https://doi.org/10.1016/j.fuel.2023.129056.
[48] Huang Ting, Xiaojia Xue, Bo Kang, et al., Influence of non-uniform pore pressure field on fracture propagation during refracturing, Block Oil Gas Field 30 (3) (2023) 475–479, https://doi.org/10.6056/dkyqt202303015, 522.
[49] Xiao Hui, Tao Hongsheng, Qiao Hongjun, Jingfu Mu, Dong Sha, Study on influence of mud pollution on formation fracture pressure, 2015 2nd Int. Conf. Eng. Technol. Appl. 22 (5) (2015) 04022, https://doi.org/10.1051/matecconf/20152204022. Fujian, China.
[50] Wenlong Ding, Tianshun Liu, Zicheng Cao, et al., Current research status and development trends of fault sealing, Petrol. Geol. Exp. 46 (4) (2024) 647–663, https://doi.org/10.11781/sysydz202404647.
[51] Xiaopeng Yan, Yili Kang, You Lijun, Xu Chengyuan, Chong Lin, Jingyi Zhang, Drill-in fluid loss mechanisms in brittle gas shale: a case study in the Longmaxi Formation, Sichuan Basin, China, JPSE 174 (2019) 394–405, https://doi.org/10.1016/j.petrol.2018.11.026.
[52] Shu He, Lixi Liang, Yinjin Zeng, et al., The influence of water-based drilling fluid on mechanical property of shale and the wellbore stability, Petroleum 2 (1) (2016) 61–66, https://doi.org/10.1016/j.petlm.2015.12.002.
[53] Ong Siong Guan, Raoof Gholami, Arshad Raza, et al., A nano-particle based approach to improve filtration control of water based muds under high pressure high temperature conditions, Petroleum 6 (1) (2020) 43–52, https://doi.org/10.1016/j.petlm.2018.10.006.